JOURNAL OF MATERIALS SCIENCE 30 (1995) 6161–6170

Hot sodium sulphate corrosion of a Nicalon silicon carbide fibre-reinforced lithium aluminosilicate glass–ceramic matrix composite

A. G. FOX, R. K. HUNT, L. C. MALDIA
Materials Science Section, Department of Mechanical Engineering, United States Naval Postgraduate School, Monterey, CA 93943, USA

S. W. WANG
Code 6063, Aircraft Division, Naval Air Warfare Center, Warminster, PA 18974, USA

The corrosion products arising from the exposure of a Nicalon silicon carbide fibre-reinforced lithium aluminosilicate glass–ceramic matrix composite to molten sodium sulphate at 900 °C for 100 h in both oxygen and argon atmospheres were studied by X-ray diffraction (XRD) and scanning and transmission electron microscopy (SEM and TEM respectively). The microstructure of the as-received composite plates was found to be similar to that reported by other workers. The matrix consisted of grains of close to stoichiometric mullite and β-spodumene and a high silica glass with 20–50 nm wide fibre–matrix interfaces comprising a layer of turbostratic carbon and amorphous silica. The effects of hot sodium sulphate corrosion were found to be very similar in both argon and oxygen but proceeded at a much greater rate in the latter case where it had progressed 100 μm into the composite and consumed many fibres. XRD studies indicated that mullite had virtually disappeared in the corroded region and this was confirmed by SEM. TEM studies of thin sections cut from near the end of the corroded zone also showed that the matrix had become a very fine mixture of glass and β-spodumene grains and that the fibre–matrix interface region had grown to ca. 600–800 nm wide. The microstructure of this corroded interface comprised several alternating layers of turbostratic carbon, mixed carbon and amorphous silica and pure carbon, each with widths varying between ca. 100 and 200 nm. This layered structure apparently developed as a result of oxidation of the silicon carbide fibre in the presence of a gradient of oxygen partial pressure that decreased from the matrix across the interface to the fibre.

1. Introduction

Ceramic matrix composites (CMC) are materials in which the aim is to produce strong, tough, damage-tolerant microstructures by the incorporation into a suitable matrix of second phases in the form of particles, whiskers, platelets or continuous fibres. In comparison with the unreinforced matrices, a number of toughening mechanisms such as transformation toughening, crack deflection, the incorporation of matrix compressive residual stresses, crack bridging and fibre pull-out can be used to increase the energy demands of the cracks as they propagate.

Examples of CMC which have been developed on a commercial scale in the last decade are zirconia-toughened alumina and silicon carbide whisker-reinforced alumina. However, in principle, it is continuous fibre-reinforced ceramics, rather than particulate-reinforced ceramics, in which the most dramatic improvements in damage tolerance can be achieved. Toughening of these materials arises from a combination of matrix crack bridging by intact fibres once an external stress necessary to initiate multiple cracking in the matrix has been applied parallel to the length of the fibres and fibre pull-out beyond the peak in the load–deflection curve for such materials (see, for example, Refs 1 and 2).

The ability of these toughening mechanisms to operate successfully depends on matrix–fibre interfaces that are relatively weak in shear to allow debonding once multiple matrix cracks begin to propagate, yet strong enough to effect good load transfer between the fibre and the matrix. Equally important is a high retained mean strength of the fibres after consolidation and environmental exposure of the composites so that the work of pull-out is as high as possible. Thus, an understanding of how a composite microstructure evolves during processing and after specific post-processing treatments, particularly in the vicinity of the matrix–fibre interface, and how this relates to mechanical properties, is vitally important in both the design and manufacturing reproducibility of these materials.

0022–2461

2. Summary of previous work on CMC fibre–matrix interfaces and environmental effects

SiC fibre-reinforced glass–ceramic composites are serious candidates for high temperature gas turbine components and so optimizing the strength–toughness behaviour of these materials by "engineering" the fibre–matrix interface is a critical area of research for the Department of Defense and the US Navy. Pioneering work by Brennan and Prewo [3] and Prewo [4, 5] has shown that SiC fibre-reinforced lithium aluminosilicates have high strength and show composite-like failure. CMC based on other glass–ceramics, such as calcium aluminosilicate (CAS), magnesium aluminosilicate (MAS) and barium magnesium aluminosilicate (BMAS) have been studied by a number of researchers [6–12]. All these CMC are tough and strong and recent work by Kumar and Knowles [12] has shown that a common feature of these composites is the presence of a thin layer of carbon at the interface between the SiC fibres and the matrix. Kumar and Knowles were further able to show that if this carbon is present in turbostratic form with its basal planes parallel to the interface then this is an arrangement favourable for matrix crack deflection and matrix–fibre debonding when suitably high tensile stresses are applied along the length of the fibres. This means that such composites will be both strong and tough.

The chemical reactions that occur during processing and which lead to carbon-rich interfacial layers which give good composite behaviour are far from being properly understood, although Cooper and Chyung [13] indicate that carbon-containing interface layers are formed as a reaction product of the oxidation of the SiC at the surface of the fibres during processing through the chemical reaction

$$SiC(s) + O_2(g) \rightarrow SiO_2(s) + C(s) \quad (1)$$

The activity of oxygen at the interface is presumed to be sufficiently low to prevent oxidation of the carbon once it has formed. The silica formed in this reaction either dissolves in the silica-rich matrix as discussed by Chaim and Heuer [14], or remains as a second layer at the interface [15]. It is also possible that some of the carbon in the interface layers arises from excess carbon present in the non-stoichiometric fibres [13, 15].

Although the formation of a carbon-rich layer at the interface between fibre and matrix is usually considered to be desirable, as it allows matrix–fibre debonding in preference to fibre failure in the composite, it is too simplistic to associate the formation of a carbon layer with "good" composite behaviour. As discussed above, it would seem that the formation of an interfacial layer of turbostratic carbon in SiC fibre-reinforced CAS, MAS and BMAS is responsible for good properties. However, in their studies of SiC fibre-reinforced pyrex, Knowles *et al.* [16] were able to show that interface layers of amorphous carbon were present in both weak and brittle, and strong and tough versions of this composite. They also demonstrated that there was clear evidence for interdiffusion of matrix and fibre elements on a micrometre scale in the brittle material but not in the tough material, and that such variations depend on prior processing history and heat treatment of both the fibre and the matrix.

Thus, it is apparent that the precise microstructure and chemistry of fibre–matrix interface layers is of vital importance. Ponthieu *et al.* [17] observed that there were differences between the high resolution electron microscope (HREM) images from interfacial layers in SiC fibre-reinforced LAS with and without Nb_2O_5 in the matrix. They also suggested that the term "amorphous carbon" to describe an interface layer is too general and that there are subtle changes in the chemistry through the interface layers and subtle differences in bonding at the matrix–layer interfaces from one composite to another, which will determine the debond resistance of the fibre–matrix interfaces.

As mentioned above and discussed by Bonney and Cooper [15], the conditions under which different forms of interfacial carbon occur are unclear. The correlation between processing history and interfacial chemistry is obviously very important and the challenge for electron microscopists is to clearly define the crystallographic/amorphous nature of the phases in the matrix, interface and fibre and correlate this with prior processing history and mechanical properties.

The effect of service environments on the interfacial chemistry of SiC fibre-reinforced glass–ceramic composites has thus far only received limited attention. An example has been described by Bischoff *et al.* [18], who showed that annealing of SiC fibre-reinforced Nb_2O_5-containing LAS for only a few hours in air at 800 °C caused the carbon interface layer to be oxidized and replaced by a silica layer, which bonds well with both the fibre and the matrix. This has the effect of making the composite brittle rather than damage tolerant. In this work we are interested in the effect of corrosion of Nicalon SiC fibre-reinforced LAS, which is a candidate for high temperature gas turbine components in aero-engines. This is because the service environment for Navy aircraft is very hostile as high-temperature components are exposed to corrodants in jet fuel and sea air that can lead to accelerated corrosion. In particular, salt deposits on hot engine components can lead to hot corrosion attack.

Although the effect of hot salt corrosion on the interface morphology of SiC fibre-reinforced CMC has not yet been extensively investigated, Jacobsen [19] has made an in-depth study of the effects of oxidation and hot corrosion of silicon carbide and other silicon-based ceramics. It is well known that, in a marine operating environment, airborne contaminants (containing salt) can combine with sulphur impurities in gas turbine combustion gases to form sodium sulphate

$$2NaCl(g) + SO_2(g) + 0.5O_2(g) + H_2O \rightarrow Na_2SO_4(l) + 2HCl(g) \quad (2)$$

Sodium sulphate is one of the most common deposits formed on structural components operated in combustion gas atmospheres. It is highly stable, generally

acidic and is usually considered to be corrosive between its melting temperature and the dewpoint at which Na_2SO_4 deposits form [19]. The range of temperatures and pressures over which sodium sulphate deposits form is, of course, a very important consideration in engine design, especially in deciding what materials to use for different components.

SiC reinforcing fibres are inherently unstable in atmospheric air and form a thin protective layer of SiO_2 which has a very low permeability to oxygen, and thus serves as an effective oxidation barrier by restricting the flow of oxygen to the SiC–SiO_2 interface. The effectiveness of the layer is limited by its melting point (2000 K) when the SiO_2 is liquefied and molecular transport and oxidation rates increase dramatically. It is possible for oxygen to get to the SiC–SiO_2 interface by the diffusion of molecular oxygen or by the network exchange of ionic oxygen. Because the diffusion rate of molecular oxygen through the amorphous SiO_2 layer is about 10^6 times faster than the ionic oxygen the former diffusion mechanism dominates [19]. Additionally, at elevated temperatures the SiC fibre and SiO_2 could react to form SiO and CO gas, which would then generate a gas pressure at the interface [19]. It is, however, generally accepted that the oxidation of SiC fibres occurs according to Equation 1 and can be broken down into five steps: (1) the transport of molecular oxygen to the SiO_2 surface; (2) the diffusion of oxygen through the SiO_2 layer; (3) reaction at the SiO_2–SiC interface; (4) the transport of the by-product gases through the SiO_2 film; and (5) the transport of by-product gases from the SiO_2 surface [19].

The key chemical reactions in the hot corrosion of silicon carbide by sodium sulphate are thus

$$SiC(s) + 1.5O_2(g) \rightarrow SiO_2(s) + CO(g) \quad (3)$$

$$xSiO_2(s) + Na_2SO_4(l) \rightarrow Na_2O \cdot xSiO_2(l) + SO_3(g) \quad (4)$$

The protective SiO_2 solid layer is thus transformed into a liquid which accelerates corrosive attack since oxygen (or oxygen-containing molecules such as H_2O) can more easily diffuse through to the SiC–SiO_2 interface. In order for Reaction 4 to occur the sodium sulphate must be basic and thus the partial pressure of the SO_3 (P_{SO_3}) plays an important role in controlling the formation of sodium silicate. Na_2SO_4 will be a basic molten salt when it has a high activity of Na_2O resulting from a low P_{SO_3}. At higher P_{SO_3}, Na_2SO_4 is acidic and will not react with acidic SiO_2. Jacobsen [19] verified these predictions by treating test coupons of SiC in a burner rig using both low- and high-sulphur fuels. More corrosion was observed on samples exposed to low-sulphur fuels (low P_{SO_3}) than those exposed to high-sulphur fuels. Additionally, no sodium silicate was detected in the coupons exposed to the high-sulphur fuels.

Many types of SiC fibres have excess carbon, some oxygen and a non-homogeneous distribution of Si, C and O through fibre cross-sections. In particular, the carbon content of the fibres can come close to 100% near fibre surfaces [9]. Carbon tends to drive sodium sulphate basic so that, even in conditions where P_{SO_3} is high enough to prevent sodium silicate formation, corrosion can still be extensive. Oxygen partial pressure is another factor that influences the hot corrosion process. It has been shown that high oxygen pressure drives sodium sulphate acidic enough that dissolution of silica does not occur. This discussion emphasizes the fact that it is extremely difficult to predict the nature of hot corrosion of silicon carbide fibre-reinforced CMC, although it is possible to speculate on its nature. In the case of SiC fibre-reinforced LAS both the surface of the SiC fibres the glassy portion of glass–ceramic matrix are high in silica, and thus likely to be acidic and so both could react with sodium sulphate if it is sufficiently basic. For this glass–ceramic matrix composite, then, hot corrosion could be extremely deleterious since it seems likely that both the SiC fibre and the matrix could be attacked by liquid sodium sulphate.

In this work the hot corrosion of Nicalon silicon carbide fibre-reinforced LAS, after exposure to molten sodium sulphate at 900 °C under different partial pressures of oxygen, was investigated. The preliminary results of this study have been published by Wang *et al.* [20].

3. Experimental procedure

A 2 mm thick 90–0–90 cross-ply plate of Nicalon silicon carbide fibre-reinforced LAS was supplied by United Technologies Research Center, East Hartford, CT. The composition of the matrix was given as (in wt %): Li_2O, 3.2; Al_2O_3, 20.0; SiO_2, 67.5; MgO, 2.5; BaO, 1.2; As_2O_3, 1.0; B_2O_3, 3.1; ZrO_2, 1.5. The final recrystallization heat treatment after hot pressing was 900 °C for 24 h. Five samples were prepared for examination: (1) as-received; (2) annealed in pure argon for 100 h at 900 °C; (3) annealed in pure flowing oxygen for 100 h at 900 °C; (4) annealed in pure argon with a surface sodium sulphate coating of 3 mg cm^{-2} for 100 h 900 °C; and (5) annealed in pure flowing oxygen with a surface sodium sulphate coating of 3 mg cm^{-2} for 100 hours 900 °C. The crystal phases present in each of these samples were investigated by X-ray diffraction (XRD). For samples (4) and (5) diffractograms were generated both before and after the excess salt had been removed from the surfaces by gentle grinding on 1200 grit SiC papers. The instrument used was a Philips PW1710 X-ray diffractometer with a Cu target and bent graphite crystal monochromator controlled with a VAX·3100 workstation. Diffractograms were obtained from the angular range of 10–90° 2θ with a step size of 0.02° and dwell time of 5 s. Cross-sections were cut at right angles to the axes of the fibres next to the exposed surfaces and these were coated in carbon and examined using backscattered electron (BSE) imaging and light element energy dispersive X-ray analysis (EDX) in a Cambridge S200 scanning electron microscope (SEM). Sections, 100 μm thick, were then cut parallel to the exposed surfaces and 3 mm diameter discs cut from them with a VCR Group model 7100 Precision Coring tool. These discs were then dimpled to ca. 25 μm thickness

using a GATAN Model 656 Dimple-Grinder and final thinning to perforation was performed in a GATAN Model 600 Duomill ion miller. Care was taken during dimpling to ensure that the thin areas were in corroded regions in the case of samples (3)–(5). The thinned discs were then examined in a JEOL 100 CX transmission electron microscope (TEM) equipped with a light element EDX operating at 120 kV.

4. Results and discussion

4.1. X-ray diffraction

Low-angle diffractograms from all the samples are shown in Fig. 1. Peaks at higher angles were found to be small and often highly broadened, and thus not useful for accurate phase identification. The major crystalline phases present in the matrix of the as-received sample are mullite, $3Al_2O_3 \cdot SiO_2$, and β-spodumene, $Li_2O \cdot Al_2O_3 \cdot 4SiO_2$. The crystalline peaks are superimposed on a background containing a glassy "hump" in the angular range 20–30°, 2θ, consistent with significant amounts of silica-based glass. There are also other peaks associated with trace phases but it is difficult to be definitive about their origin. There is also the possibility of preferred orientation which would also make identification of trace phases difficult. At higher angles β-silicon carbide from the fibres was also detected but the peaks were small and highly broadened due to the small size of the β-SiC crystallites. Any other phases in this sample were evidently present in small amounts as they could not be detected by XRD.

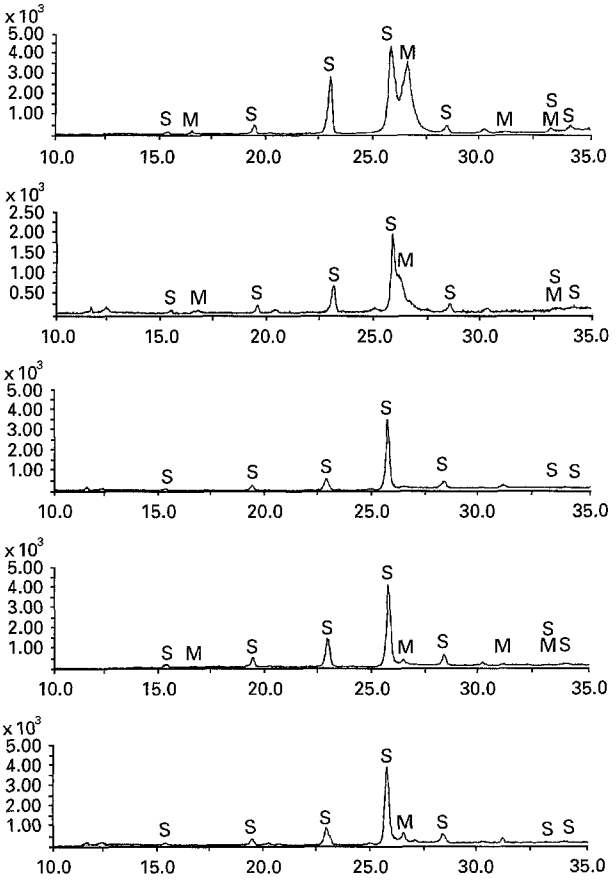

Figure 1 X-ray diffractograms of the five samples studied in the present work. The results are presented in the following order (from top to bottom): as-received, annealed in argon, annealed in argon with a sodium sulphate coating, annealed in flowing oxygen and annealed in flowing oxygen with a sodium sulphate coating. S = β-Spodumene and M = mullite.

The diffractogram for the sample annealed in argon without a salt coating also shows β-spodumene and -mullite as the major crystalline phases, although the amount of the latter has been markedly reduced and the amount of glass appears to have increased somewhat since the intensities of the crystalline peaks have been reduced and the glassy "hump" seems somewhat larger; this would suggest that the Al_2O_3 contents of the glass and β-spodumene have also been increased. In addition, there is also evidence for trace amounts of β-eucryptite, $Li_2O \cdot Al_2O_3 \cdot 2SiO_2$, in this sample. Annealing in argon with a salt coating produces similar results except that mullite is reduced to trace amounts. According to the Li_2O–SiO_2–Al_2O_3 ternary phase diagram this behaviour is consistent with the overall composition of the matrix approaching equilibrium and that this takes place more quickly when sodium sulphate is present.

XRD of the sample annealed in flowing oxygen once again showed β-spodumene and glass to be the predominant phases present, and once again the mullite had almost completely disappeared. Trace amounts of clineoenstatite, $MgO \cdot SiO_2$, are now evident but there is little evidence for β-eucryptite. In addition, there is also some evidence for low quartz. Annealing in oxygen with a sodium sulphate coating produced similar results except for the return of evidence for trace amounts of β-eucryptite.

Although the phases present after various heat treatment/corrosion regimes can be determined by XRD it reveals very little about the possible extent and mechanism of corrosion. SEM and TEM experiments are necessary for this. These results will now be presented.

4.2. Scanning electron microscopy

Fig. 2 is a BSE SEM micrograph of the as-received sample clearly showing the fibres and matrix. The

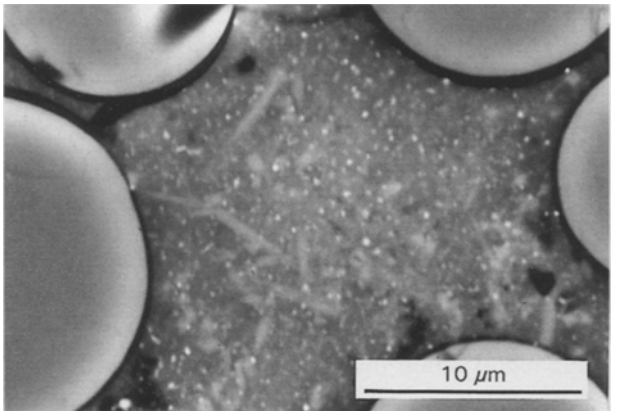

Figure 2 Backscattered SEM micrograph of the as-received sample showing fibres, matrix, mullite with acicular morphology and bright particles containing zirconia and sometimes small amounts of arsenic oxide and/or magnesia.

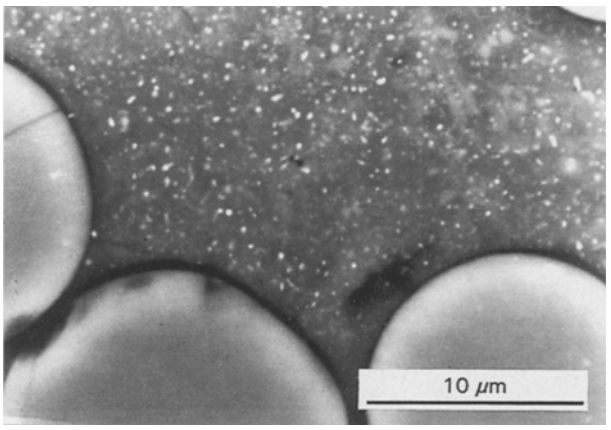

Figure 3 Backscattered SEM micrograph of the sample annealed in argon with no sodium sulphate coating. This is very similar to Fig. 2 except there is a marked reduction in the amount of mullite present.

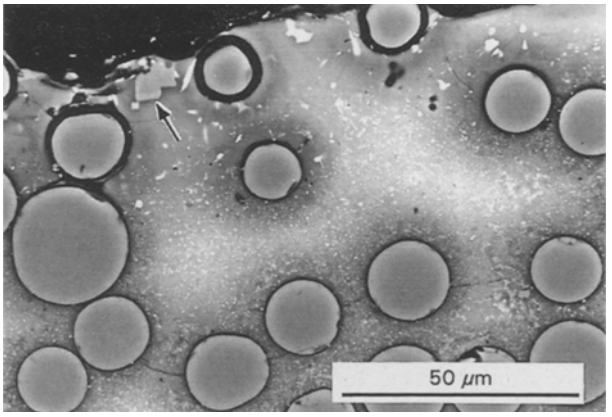

Figure 4 Backscattered SEM micrograph of the sample annealed in argon with a sodium sulphate coating. The corrosion zone extends ca. 20 μm into the specimen and in this region the fibres have been attacked and there is apparently a complete absence of mullite. The particle arrowed was analysed by EDX to be stoichiometric $MgO{\cdot}SiO_2$.

matrix apparently contains several phases of differing average atomic number. The acicular phase, which evidently has a higher average atomic number than the matrix as a whole, was found by EDX analysis to be close to stoichiometric mullite in agreement with the XRD data. The darker matrix regions in this micrograph must evidently be a mixture of glass and β-spodumene; it was difficult to discriminate between these in the SEM. Bright (high average atomic number) particles associated with ZrO_2 and occasionally As_2O_3 and/or MgO are also present. No evidence for BaO or its compounds was found in the regions examined in the SEM.

SEM studies of the sample annealed in argon without a salt coating showed no evidence of corrosion and the high magnification BSE micrograph (Fig. 3) clearly shows a much lower matrix mullite content compared with the equivalent micrograph taken from the as-received sample (Fig. 2). Once again there was clear evidence for ZrO_2 and As_2O_3/MgO-containing particles as in the as-received specimen. Annealing in argon with a salt coating caused degradation of the fibres near the surface, as shown in Fig. 4, and the disappearance of mullite in agreement with the XRD experiments. The large arrowed particle in this figure was found by EDX to be close to stoichiometric magnesium silicate, $MgO{\cdot}SiO_2$, which, of course, is consistent with the detection of clineoenstatite by XRD for this sample; several other particles of this type were identified near the surface in this sample. The fibres within ca. 20 μm of the surface appear to have been oxidized and the origin of the oxygen causing this is not clear. The argon used in the experiments was designated oxygen-free and, if this is the case, the only possible source of oxygen for corrosion is thennardite, Na_2SO_4. The nature of any possible dissociation of the thennardite is not clear. Simplistically, a reaction of the form $2Na_2SO_4 \rightarrow 2Na_2SO_3 + O_2$ could be expected. However, the XRD of the corroded, coated and unpolished samples failed to display evidence of sodium sulphite. These diffractograms contained peaks from phases other than mullite, β-spodumene and thennardite which were not present in the polished samples, and thus could have been a result of a dissociation process. As yet we have been unable to identify these phase(s) and they do not appear to be listed in the Joint Commission on Powder Diffraction (JCPDS) files. It is clear that oxygen was available for corrosion and that this reacted with the β-SiC during annealing to form SiO_2. Apparently, this excess SiO_2 subsequently reacted with nearby MgO to form clineoenstatite. EDX of all the corroded regions near the surface (except the salt layer) failed to detect any sulphur or sodium which suggests that any dissociation of the Na_2SO_4 was such that the sodium and sulphur were confined to the salt layer and that only released oxygen reacted with the SiC fibre-reinforced LAS. In addition, the fact that magnesium silicate is present in the surface regions next to the salt layer indicates that sodium and sulphur have remained in the salt coating and not taken part in the corrosion process since, if free Na_2O was present, sodium silicate would be more likely to form than magnesium silicate, as Na_2O is significantly more basic than MgO.

The XRD shown in Fig. 1 are very similar for the sample annealed in argon with a salt coating and for the sample annealed in oxygen without a salt coating. SEM micrographs of these two samples also show similarities as can be seen from a comparison of Figs 4 and 5 which are BSE SEM micrographs of the surface corroded regions in these specimens. In the case of the sample annealed in oxygen, the corrosion zone extends somewhat more into the sample, to a depth of ca. 30 μm, and all the fibres in this region have the appearance of being oxidized. Once again, no sulphur or sodium was found in the corrosion zone and there is an almost total absence of mullite with clearly visible particles of the corrosion product magnesium silicate. In addition, in Fig. 5, there is evidence of a corrosion product around the partially oxidized fibres which is most likely to be SiO_2 and is difficult to analyse by EDX because of its small size, and much of it apparently fell out during specimen preparation. Notice also the significant number of pores in the regions near the oxidized fibres which suggests that carbon monoxide was generated during the oxidation

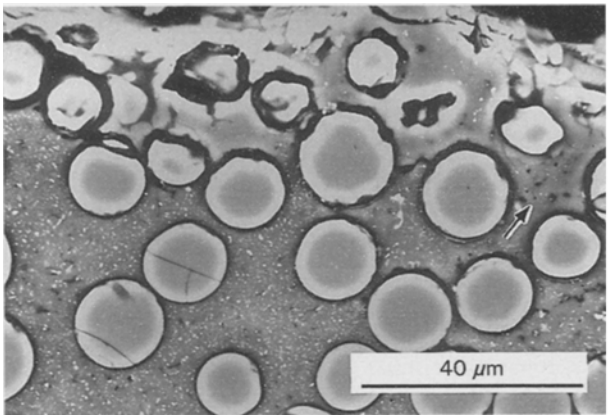

Figure 5 Backscattered SEM micrograph of the sample annealed in flowing oxygen with no sodium sulphate coating. The corrosion zone extends ca. 30 μm into the specimen and there is a complete absence of mullite. Magnesium silicate particles are in evidence in the corroded region; these appear somewhat overbright due to topographical effects which apparently arose from surface damage generated during sample preparation. Notice the presence of porosity around some of the oxidized fibres (arrowed).

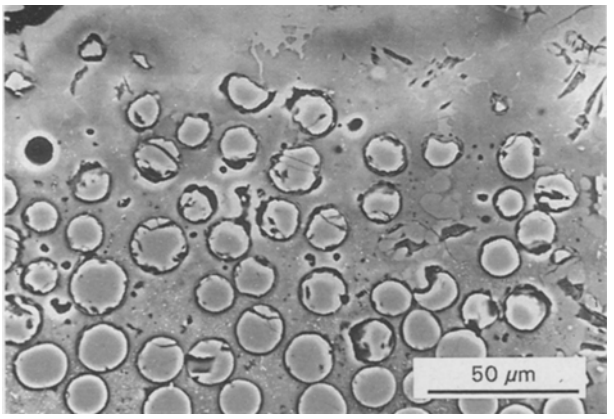

Figure 6 Backscattered SEM micrograph of the sample annealed in flowing oxygen with a sodium sulphate coating. The corrosion zone extends ca. 100 μm into the specimen and there is a complete absence of mullite. Once again, magnesium silicate particles and porosity are evident in the corroded region.

of the silicon carbide fibres. Fig. 6 is a BSE SEM micrograph of the corrosion zone of the sample heat treated in oxygen with a sodium sulphate coating and, in this case, the corrosion zone extends into the sample by ca. 100 μm. Once again, no sodium or sulphur was found in the corroded region but it is clear that sodium sulphate accelerates the oxidation process since the corrosion zone is much larger than for the sample annealed in oxygen without salt. As before, notice the absence of mullite and the presence of large numbers of pores around oxidized fibres and clearly visible particles of magnesium silicate. In this sample it was possible to find oxidized fibres with clearly preserved rings of oxidation product as shown in Fig. 7. EDX analysis of these suggested that they are comprised mostly silica with a small amount of alumina.

4.3. Transmission electron microscopy

TEM imaging, selected area diffraction (SAD) and EDX studies of the as-received matrix indicated that it

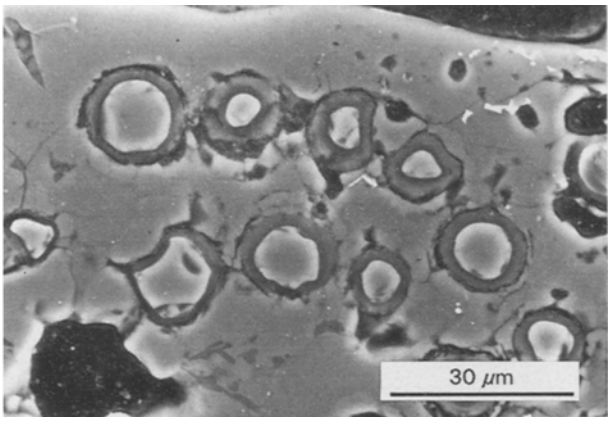

Figure 7 Backscattered SEM micrograph of the sample annealed in flowing oxygen with a sodium sulphate coating showing the corroded fibres. The "ring" of corrosion product around the fibres was found by EDX to be mostly silica with a small amount of alumina. Porosity is again evident near these corroded fibres.

comprised close to stoichiometric mullite with widely varying grain sizes in agreement with the SEM observations and close to stoichiometric β-spodumene with grain sizes in the range 0.5–2.0 μm. These were surrounded by amorphous glassy regions with average composition (by weight) of SiO_2, 88% – Al_2O_3, 12% (with trace amounts of BaO and As_2O_3); this analysis ignores the possible presence of Li_2O which cannot be detected by EDX. Small ZrO_2 and MgO crystallites were also observed and the former sometimes contained As_2O_3. These crystallites were found predominantly in the glassy regions with very few observed in the crystalline grains. In the limited area examined in the TEM no evidence for B_2O_3 or its compounds was found, which is not surprising since it is very difficult to analyse boron using EDX. The amorphous glassy phase dominated the matrix component of the matrix–fibre interfaces in the areas studied in the present work and an example is shown in Fig. 8. The fibre region next to the interface was found to be predominantly amorphous carbon containing silicon and some oxygen and very few β-SiC particles. A small amount of alumina was detected by EDX in this fibre region next to the interface suggesting that diffusion of Al (and possibly Li also) from the matrix into the fibre had taken place during processing, although the sample is quite thick here and thus beam broadening may have meant that the matrix was contributing to this analysis. A selected area diffraction pattern taken from the interface, which is also shown in Fig. 8, shows faint rings due to graphitic carbon superimposed on an amorphous background. Dark-field imaging of several interfaces (see, for example, Fig. 9), using the 0 0 2 carbon ring, showed that the very low atomic number interface layer with a width in the range 20–50 nm and which is clearly evident in Figs 8 and 9, is graphitic carbon which appears to be mixed with amorphous silica. The presence of the 0 0 2 and $hk0$ reflections and the absence of the hkl reflections (except 0 0 2) in this ring pattern suggests that this carbon layer is turbostratic [21]. Using high-resolution electron microscopy, Kumar and Knowles [12] have

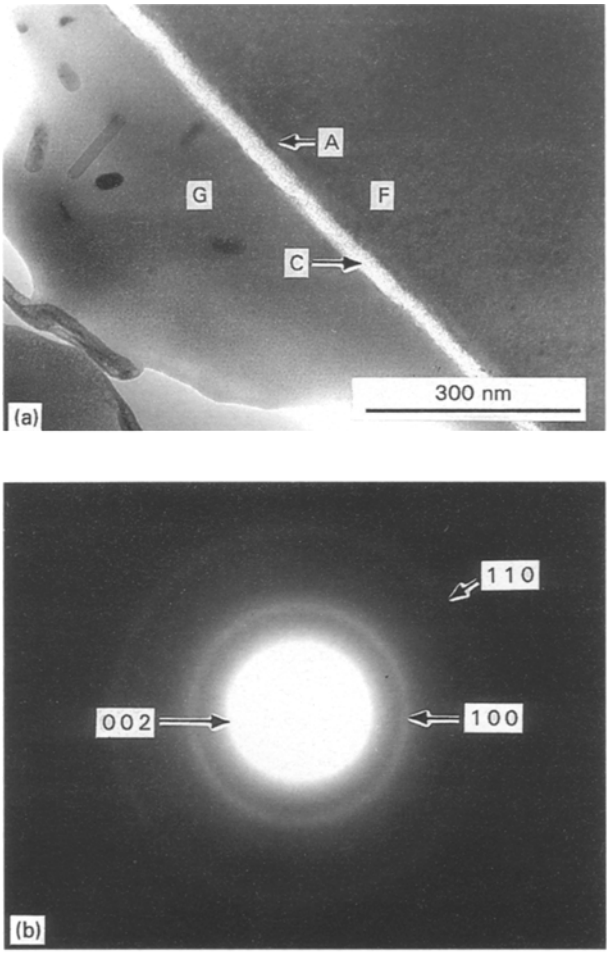

Figure 8 Bright-field TEM micrograph (a) and selected area diffraction pattern (b) from an interface in the as-received sample. ZrO_2- and MgO-containing precipitates are clearly seen in the amorphous glassy matrix next to the interface and the fibre region next to the interface is dominated by amorphous silicon oxycarbide with only a few small particles of β-silicon carbide. The indexed diffraction pattern from the interface is consistent with rings from turbostratic carbon (C) superimposed on an amorphous background which arises partly from the matrix glass (G), partly from the amorphous silicon oxycarbide region of the fibre (F) and partly from the amorphous silica layer (A) at the interface.

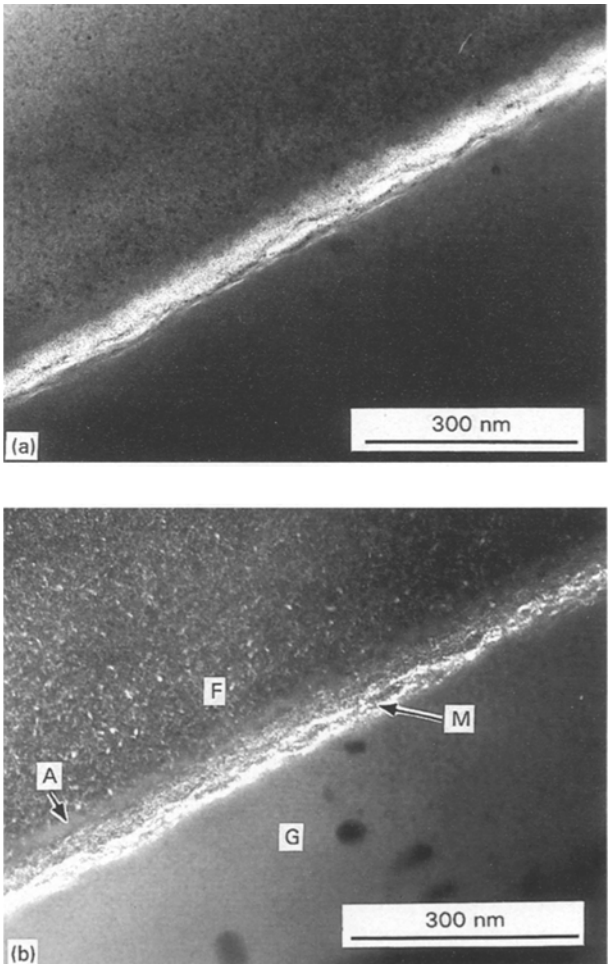

Figure 9 Bright-field (a) and dark-field (b) TEM micrographs of an interface in the as-received sample. The dark-field micrograph was taken using the 002 turbostratic carbon reflection and clearly shows the mixed turbostratic carbon–amorphous silica layer (M) alongside a thin amorphous silica layer (A). The fibre (F) and the glassy matrix (G) are also indicated.

shown that such interfacial carbon layers in MAS are indeed turbostratic with the basal planes parallel to the fibre axes. Also evident in Figs 8 and 9 is a second interfacial layer with a width of the order of 100 nm; this was identified by EDX and SAD to be amorphous silica containing trace amounts of alumina. Finally, TEM bright- and dark-field imaging, and SAD of the interior of the Nicalon fibres showed them to be small (2–3 nm) crystals of β-SiC in an amorphous carbon-rich silicon carbide matrix, as has been reported previously by many other workers. These results are very similar to those obtained by Chaim and Heuer [14] and Cooper and Chyung [13] discussed in section 2.

In the thin areas of the sample annealed in argon without a salt coating studied in the TEM no mullite was detected and the alumina content of both the glass and β-spodumene was increased; in addition, grains of stoichiometric β-eucryptite were occasionally observed, consistent with the XRD observations. The average composition (by weight) of the glassy regions was now found by EDX to be SiO_2, 84%–Al_2O_3 16% (once again ignoring Li_2O). A similar increase in the alumina content of the β-spodumene (cf. the as-received sample) was also detected. As mentioned previously, the constitution of the matrix after annealing in argon is entirely consistent with progression towards equilibrium according to the Li_2O–Al_2O_3–SiO_2 phase diagram. TEM examination of the morphology of the interface regions suggested that these were unchanged by annealing in argon with all the features being almost identical to those observed in the as-received specimen.

Since the corrosion products appeared to be the same for the three samples that experienced oxidation it was decided to perform TEM studies on the sample with the largest corroded region (heat treated in oxygen with a sodium sulphate coating) since preparing accurately positioned samples in corroded regions 20–40 μm thick proved problematical. In the case of the sample heat treated in oxygen with a sodium sulphate coating it proved possible to prepare a thin section close to the border between the corroded and uncorroded regions. TEM examination of the corroded matrix revealed a fine mixture of small crystallites

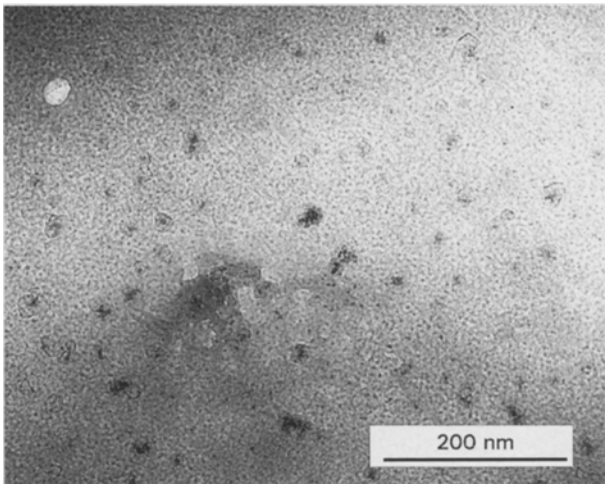

Figure 10 Bright-field TEM micrograph of the matrix in the corroded region of the sample annealed in flowing oxygen with a salt coating. The microstructure is a mixture of fine crystallites of β-spodumene and amorphous glass.

surrounded by glass, as shown in Fig. 10. Selected area diffraction showed the crystallites to be β-spodumene, in agreement with the X-ray data obtained from this sample. Very few MgO crystallites were found in the thin areas studied in this specimen since they had no doubt diffused away to form $MgO{\cdot}SiO_2$. Some ZrO_2 crystallites were, however, still present, although they now appeared several times larger than in the as-received sample. EDX analyses of all the phases present in the matrix, fibre and interface failed to reveal the presence of any sodium, once again suggesting that conditions were insufficiently basic for the dissociation of the sodium sulphate coating. TEM studies of the fibre–matrix interface showed these to be extensively corroded as shown in Fig. 11. In the as-received sample the interfacial region comprised a 20–50 nm layer of turbostratic carbon and a ca. 100 nm thick amorphous SiO_2 layer. Fig. 11 indicates that interfacial regions can grow to between 600 and 800 nm due to oxidation and have a very interesting layered structure. Selected area diffraction from this layered region produced a ring pattern consistent with turbostratic carbon superimposed on an amorphous background. A dark-field image obtained from the 002 carbon ring is also shown in Fig. 11. EDX and SAD analyses of the carbon-free interfacial layers (darker in the bright-field image of Fig. 11) showed them to be amorphous silica containing a small amount of alumina which had evidently diffused into the interface region from the matrix. The carbon-containing layer next to uncorroded fibre is clearly a mixture of silica and carbon, and studies of several interfaces showed that a mixed carbon/amorphous silica layer was always present in the corroded interface region next to the uncorroded fibre. The carbon-rich interlayer marked "C" in Fig. 11 appears to contain very little silica and the layer next to the matrix appears to be predominantly amorphous silica, although there is faint evidence for a carbon layer next to the matrix which was probably burned-out by oxidation and replaced by amorphous silica which expands on

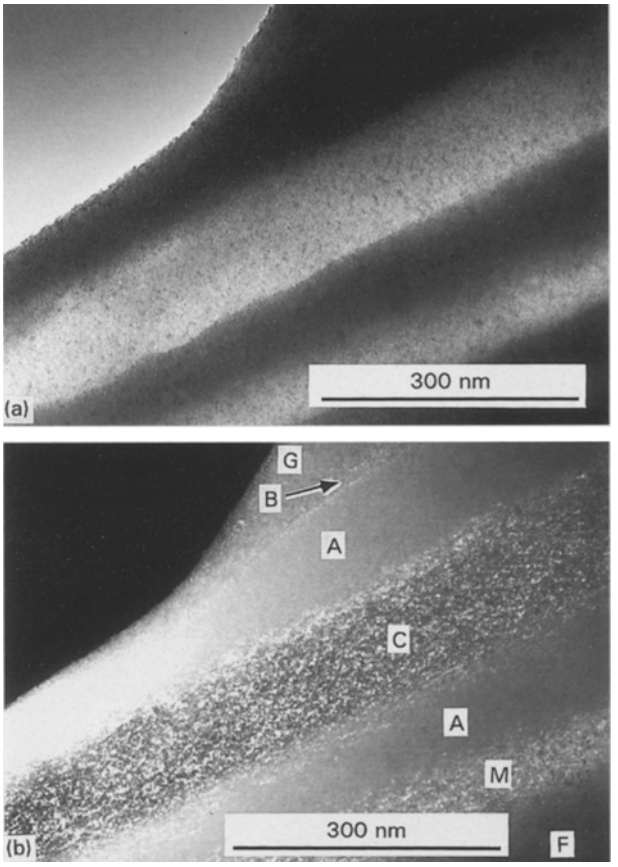

Figure 11 Bright-field (a) and dark-field (b) TEM micrographs of a corroded interface region in the sample annealed in flowing oxygen with a salt coating. In the dark-field image, which was taken using the 002 turbostratic carbon reflection, notice the layered structure of amorphous silica mixed with turbostratic carbon (M), amorphous silica (A), turbostratic carbon (C) and carbon burn-out region (B) between the glass matrix (G) and the fibre (F).

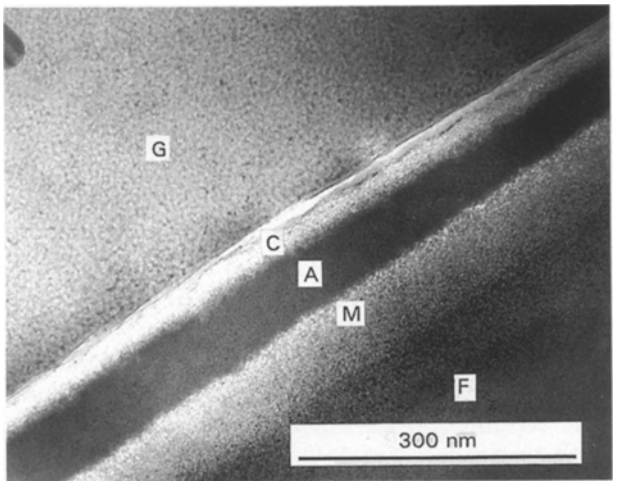

Figure 12 Bright-field TEM micrograph of a corroded interface in the sample annealed in flowing oxygen with a salt coating. The features in the interface are labelled in the same manner as Fig. 11.

formation. Other layered interfaces investigated in the TEM showed evidence for almost pure carbon layers adjacent to the matrix, as shown in Fig. 12.

Similar interfacial features have also been observed by Kumar and Knowles [22] in Nicalon silicon carbide fibre-reinforced MAS, and they suggested that the amorphous silica layers next to the matrix form by

the oxidation of carbon which diffuses from the mixed turbostratic carbon/amorphous silica layers towards the fibre–matrix interface. In the present work we have also observed a mixed turbostratic carbon/amorphous silica layer at the interfaces of the as-fabricated samples, as shown in Fig. 8, and so the mechanism for the generation of the interlayers proposed by Kumar and Knowles also seems appropriate here. Since the equilibrium partial pressure of oxygen for the oxidation of carbon to CO (by the reaction $2C + O_2 = 2CO$) is higher than that for the oxidation of SiC to silica and carbon by Reaction 1 (up to ca. 1500 °C), it is expected that the fibres will also be oxidized to form more silica and carbon. The presence of a mixed silica/carbon interlayer next to the fibres in all the corroded interfaces studied certainly supports this hypothesis. The existence of a burned-out carbon layer next to the matrix in Fig. 11 could certainly be a result of the oxidation of a carbon interlayer to CO gas. If this is so, a carbon layer must first form at the interface between the silica layer and the mixed carbon/silica interlayer. Carbon enrichment could then occur at this interface by the diffusion of carbon from the mixed interlayer towards the silica interlayer; the driving force for this is the concentration gradient of carbon between the two interlayers. Consequently, if the partial pressure of oxygen at this interface is higher than the equilibrium partial pressure for the oxidation of carbon to form CO, then the carbon will oxidize to form CO gas and thus a burned-out carbon layer, provided that the rate is limited by the diffusion of CO away from the interface. If the burn-out of the carbon layer is extensive, then elongated pores and voids could form. In addition, enrichment of carbon at the interface between the mixed interlayer and the pure silica layer would most likely lead to the formation of a silica-rich layer within the mixed interlayer. If this is so, then the interface layer structure could be expected to be of the form: fibre–silica + carbon–silica–C burn-out–silica–matrix or, if the oxidation is more extensive, multiple layers of the type: fibre–silica + carbon–silica–carbon–silica–C burn-out–matrix could form [22]. If the carbon burn-out is severe then interfaces with the layered structure fibre–silica + carbon–silica–pores–silica–matrix could develop. Interface morphologies of this latter type containing pores were observed by Kumar and Knowles [22] in oxidized samples of Nicalon silicon carbide fibre-reinforced MAS when the TEM samples were cut from near the surface. In the present work the TEM samples were taken near the end of the corroded zone. None the less, Fig. 11 shows a layer next to the matrix which is clearly carbon layer burn-out, and this indicates that the corroded interface in this figure could have developed by this mechanism. Evidence of CO emission and pore formation around extensively corroded fibres nearer the surface of the corroded sample can also be seen in the SEM micrograph, Fig. 7.

If, however, the partial pressure of oxygen is lower than the equilibrium partial pressure for the oxidation reaction of carbon to CO gas, then the carbon interlayer will remain stable at the interface between the mixed and the silica interlayers. The continuous oxidation of the fibres will again form a silica + carbon layer and an interface morphology of the type fibre–silica + carbon–silica–carbon–silica–matrix will be expected and this is exactly what is seen in Fig. 12 (cf. ref. 22). This argument suggests that the local oxygen activity near the interface shown in Fig. 12 is somewhat lower than that in Fig. 11, despite the fact that both interfaces were ostensibly at the same distance from the sample surface. This is supported by the observation that the extent of oxidation of the interface shown in Fig. 12 is far less than that of Fig. 11. This can be explained if one considers the possible presence of interconnected porosity, cracks and the diffusion of oxygen along the interfaces from the exposed ends of fibres (pipe-line oxidation). The existence of such easy paths for the diffusion of oxygen could certainly mean that local oxygen fluxes at fibre–matrix interfaces could vary significantly even if these interfaces are at similiar distances from the sample surface.

Our previous mechanical properties studies on Nicalon fibre-reinforced LAS exposed to sodium sulphate coatings in air at 900 °C for 100 h indicated that the tensile strength was reduced by ca. 30% and that the elastic modulus was also reduced by this corrosion regime. This is entirely consistent with the electron microscope data presented above which indicates that significant amounts of high strength, high modulus SiC fibres have been consumed by the corrosion process. In addition, the interfaces between the fibres and the matrix have been degraded by oxidation and this also undoubtedly contributed to these changes in mechanical properties.

5. Conclusions

1. When a Nicalon silicon carbide fibre-reinforced lithium aluminosilicate (LAS) glass–ceramic matrix composite is annealed in an inert atmosphere (argon) the LAS matrix appears to progress towards equilibrium and the SiC fibres and their interfaces with the matrix do not appear to be changed significantly.
2. When a Nicalon silicon carbide fibre-reinforced LAS glass–ceramic matrix composite is annealed in the presence of oxygen (emanating from either a sodium sulphate coating or an oxygen atmosphere, or both) an extensive corrosion zone is formed in which the matrix has become a fine mixture of β-spodumene crystallites and high silica glass. Exposure to oxygen appears to severely corrode the SiC fibres so that extended layered interfaces comprising amorphous silica, turbostratic carbon and mixtures of these are formed; the exact morphology of the layers depending on the local oxygen flux. Oxidation of the fibres in this way apparently leads to severe degradation of mechanical properties.

Acknowledgements

The authors would like to thank Dr A. Kumar for many interesting discussions, particularly on the topic of oxidation of silicon carbide fibre-reinforced

glass–ceramic matrix composites. This work was funded by grants from the Naval Postgraduate School, Monterey, CA, and the Naval Air Warfare Center, Warminster, PA.

References

1. J. AVESTON, G. A. COOPER and A. KELLY, in Proceedings of the Conference on Fiber Composites, NPL, Guildford UK, 1971 (IPC Science and Technology Press, London) p. 15.
2. A. G. EVANS and D. M. MARSHALL, *Acta Metall.* **37** (1989) 2567.
3. J. J. BRENNAN and K. M. PREWO, *J. Mater. Sci.* **17** (1982) 2371.
4. K. M. PREWO, *J. Mater. Sci.* **21** (1986) 3590.
5. K. M. PREWO, *Mater. Res. Soc. Proc.* **120** (1988) 145.
6. R. CHAIM, D. G. BRANDON and L. BAUM, *Ceram. Engng. Sci. Proc.* **9** (1988) 695.
7. M. Y. CHEN, J. M. BATTISON and TAI-IL MAH, *J. Mater. Sci.* **24** (1989) 3213.
8. B. J. NORMAN and B. P. TILLEY, *Proc. Brit. Ceram. Soc.* **46** (1990) 127.
9. M. H. LEWIS and V. S. R. MURTHY, *Comp. Sci. Tech.* **42** (1991) 221.
10. S. M. BLEAY, V. D. SCOTT, B. HARRIS, R. G. COOKE and F. A. HABIB, *J. Mater. Sci.* **27** (1992) 2811.
11. B. L. METCALFE, I. W. DONALD and D. J. BRADLEY, *ibid.* **27** (1992) 3075.
12. A. KUMAR and K. M. KNOWLES, *Acta Metall. Mater.* in press.
13. R. F. COOPER and K. CHYUNG, *J. Mater. Sci.* **22** (1987) 3148.
14. R. CHAIM and A. H. HEUER, *Adv. Ceram. Mater.* **2** (1987) 154.
15. L. A. BONNEY and R. F. COOPER, *J. Amer. Ceram. Soc.* **73** (1990) 2916.
16. K. M. KNOWLES, A. KUMAR and D. W. SHIN, in "Electron microscopy and analysis '91", Bristol UK, September 1991, edited by F. J. Humphreys (Institute of Physics, London). Inst. Phys. Conf. Ser. No. 119: Section 7, 261.
17. C. PONTHIEU, M. LANCIN, J. T. DESSEAU and S. VIGNESCOULT, *J. de Physique* **51** (1990) C1.
18. E. BISCHOFF, M. RUHLE, O. SBAIZERO and A. G. EVANS, *J. Amer. Ceram. Soc.* **72** (1989).
19. N. S. JACOBSEN, *J. Amer. Ceram. Soc.* **76** (1993) 3.
20. S. W. WANG, R. W. KOWALIK and R. R. SANDS, *Ceram. Engng. Sci. Proc.* **14** 385.
21. R. E. FRANKLIN, *Acta Crystallogr.* **4** (1951) 253.
22. A. KUMAR and K. M. KNOWLES, *J. Amer. Ceram. Soc.* accepted.

Received 6 March
and accepted 24 May 1995